Effect of geometry on the critical currents of thin films

G. Stejic
Department of Physics, University of Wisconsin–Madison, Madison, Wisconsin 53706

A. Gurevich
Applied Superconductivity Center, University of Wisconsin–Madison, Madison, Wisconsin 53706

E. Kadyrov
Department of Physics, University of Wisconsin–Madison, Madison, Wisconsin 53706

D. Christen
Solid State Division, Oak Ridge National Laboratory, Oak Ridge, Tennessee 37831

R. Joynt
Department of Physics, University of Wisconsin–Madison, Madison, Wisconsin 53706

D. C. Larbalestier
Applied Superconductivity Center, Department of Physics and Department of Materials Science and Engineering, University of Wisconsin–Madison, Madison, Wisconsin 53706

(Received 16 August 1993)

We consider experimentally and theoretically the effect of the thickness on the critical current density J_c of superconducting films. In order to eliminate possible contributions from intrinsic pinning, our measurements of $J_c(\varphi)$ as a function of the amplitude and orientation of the magnetic field **H** with respect to the film plane were performed on isotropic Nb-Ti films having thicknesses d ranging from $\lambda/4$ to 4λ, where λ is the London penetration depth, and $\mathbf{H}\perp\mathbf{J}$. The angular dependent $J_c(\varphi)$ has a sharp peak for **H** parallel to the film surface, similar to that observed for high-T_c films. The amplitude of the peak increases as d decreases and reaches 20–30 % of the depairing current density (J_d) for the $\lambda/2$ film. The ratio of J_c values for parallel ($J_{c\parallel}$) and perpendicular ($J_{c\perp}$) film orientation increases as d decreases, so that $J_{c\parallel} \ll J_{c\perp}$ for the 4λ film and $J_{c\parallel} \gg J_{c\perp}$ for the $\lambda/4$ film, the crossover occurring at $d \approx 2\lambda$. A proposed interpretation of these results is based on our calculations of the vortex behavior in thin ($d \ll \lambda$) films, which give analytical formulas for the field distribution around a fluxon, the lower critical field, H_{c1}, the surface barrier, and the vortex-vortex interaction potential. The film geometry gives rise to a significantly enhanced surface barrier and H_{c1}, a marked decrease of the range of the intervortex repulsion (to d instead of λ), and noncentral, position-dependent forces between vortices. These results are employed to evaluate the bulk and surface contributions to $J_{c\parallel}(d)$, both being shown to increase as d decreases. The bulk component of $J_{c\parallel}$ exhibits a $1/d^2$ dependence at $d > d_c$ due to the decrease of the tilt elastic modulus $c_{44}(d)$ of the vortex structure, a crossover from the collective to a single-vortex regime of pinning occurring below a critical thickness at $d < d_c$. The surface magnetic pinning gives the main contribution to J_c for our $\lambda/2$ and $\lambda/4$ films, leading to $J_{c\parallel}$, which increases as $1/d$ and becomes of order J_d at $H \approx H_{c1}$. These calculations show that the ratio $J_{c\parallel}(d)/J_{c\perp}(d)$ increases as d decreases, with the $J_{c\parallel}(d)/J_{c\perp}(d)$ value being much less than unity at $d \gg \lambda$ and much larger than unity at $d \ll \lambda$. The results obtained indicate that the effect of the film geometry can be very important when interpreting the angular dependences of critical currents of thin films.

I. INTRODUCTION

The critical current density J_c in superconductors is usually described in terms of two qualitatively different approaches based on either single-vortex or collective pinning models. The first model assumes that J_c is mostly determined by the direct summation of the elementary pinning forces over all vortices, the intervortex repulsion weakly affecting J_c.[1] By contrast, in the collective pinning approach, the interaction between vortices is assumed to be much stronger than their interaction with pinning centers, and the vortex structure behaves as a continuous elastic medium which is weakly distorted by a random pinning potential $U_p(\mathbf{r})$. A nonzero J_c then results from a mean-squared fluctuation of $U_p(\mathbf{r})$ over a macroscopic correlation volume $V_c = R_c^2 L_c$ whose size is determined by the competition between elastic and pinning forces.[2] In their two respective limits, the single vortex model is expected to correspond to a material having a dense structure of strong pinning centers, while a weak pinning material should be treated by the collective pinning model.

The most satisfactory approach to checking the validity of any flux pinning model is to make materials with well-defined and controlled densities of defects and then to investigate the change in J_c when the density and/or strength of the pinning is varied. Such experiments are not easy to perform, since they require control of the microstructure on the scale of the coherence length (ξ) which is below 10 nm for most high-J_c type II superconductors. Such nanometer scale microstructures (nanostructures) are often thermodynamically unstable, require very large efforts to be quantitatively described and are seldom subject to much control. As a result, it was possible to quickly understand and describe the flux pinning in low-J_c materials, for example, in the Pb-Bi system ($\xi \approx 15$ nm),[1] but took some 10–15 years longer before the flux pinning in the very important Nb-Ti system ($\xi \approx 5$ nm) could be quantified.[3] The high-temperature superconductors (HTS) exhibit these problems in an extreme way. The coherence lengths lie in the range of 0.3–1.5 nm, dimensions which are comparable to atomic sizes. Thus any crystalline disorder can in principle produce pinning; such atomic disorder is very hard to measure and control; therefore at least up until the present, modeling seems the only practical way to estimate the effect of such defects. The intrinsic anisotropy of the layered HTS itself conveys the possibility of "intrinsic pinning" by nonsuperconducting layers of the microstructure[4] and very small growth defects such as twins, stacking faults or surface steps produced by screw dislocations may pin the vortices in thin films placed in a magnetic field perpendicular to their broad face ($H_\perp$).

The present work addresses the rather general issue of what controls the critical current in thin films, as the orientation of the film plane to the magnetic field is changed and as the film thickness is varied about the penetration depth (λ). One of the motivations for the work was to address the apparent puzzle of why thin-film $YBa_2Cu_3O_{7-\delta}$ (YBCO) generally has a J_c about 1–2 orders of magnitude larger than bulk YBCO. A flux pinning analysis based on the direct summation arguments[5] leads to the conclusion that to account for the high-J_c values in thin films, the defects must be approximately coherence length in size and spaced by only 5.3 nm.

The present paper addresses the geometrical aspects of thin films, since the decrease of the sample sizes can strongly enhance J_c. For instance, numerous experiments, performed on both HTS (Refs. 6–10) and low-temperature superconductors (LTS) (see, e.g., Refs. 11 and 12) films, have shown that the J_c of thin films can considerably exceed the J_c of bulk superconductors and can be even comparable to the maximum possible value of J_c determined by the depairing current density, J_d:

$$J_d = \frac{c\phi_0}{12\sqrt{3}\pi^2\lambda^2\xi} , \tag{1}$$

where c is the speed of light and ϕ_0 is the magnetic flux quantum. In addition, there is an extensive literature on the orientational dependence of $J_c(\varphi)$ of epitaxial HTS films as a function of the angle φ between **H** and the normal to the film surface. These experiments have revealed pronounced peaks in $J_c(\varphi)$ for **H** parallel to the surface which are usually ascribed to an additional intrinsic pinning of vortices by the *ab* planes.[13–18] Similar dependencies of $J_c(\varphi)$ have been observed in multilayer superconducting superlattices.[19,20]

There are several mechanisms which could be responsible for high-J_c values in thin films, some of which such as the surface pinning caused by the step structure of screw dislocations,[21,22] or a very high density of as yet unidentified pins[5] have already been mentioned. Another more fundamental reason is due to qualitative changes in the vortex behavior as the film thickness d becomes smaller than λ, or one of the pinning correlation lengths L_c or R_c. For instance, in films placed in a perpendicular magnetic field H, there is a crossover from the three-dimensional (3D) to 2D regimes of the collective pinning, if the longitudinal pinning correlation length along the vortex line $L_c(H)$ becomes smaller than the film thickness d.[23–25] In HTS films this effect can also give rise to the significant enhancement of thermal fluctuations in the vortex structure, which can result in its melting over a significant portion of the T-H diagram.[26] In general, such a 3D→2D pinning transition is accompanied by an increase of J_c due to the drop of the correlation volume V_c.[23–25]

At the level of individual vortices, a qualitative change of the orientational field dependence of $J_c(\mathbf{H})$ occurs as the thickness d becomes smaller than λ. For instance, for a film in perpendicular field, the intervortex repulsion becomes more long-range, varying over the length $\sim\lambda^2/d$ rather than λ, as d is decreased below λ,[27] and the lower critical field H_{c1} becomes much smaller than its bulk value, due to the large demagnetization factor. By contrast, decreasing d below λ for a film in a parallel field raises H_{c1} and the thermodynamic critical field H_c due to the decrease of the magnetic flux in the vortex.[28,29] The mechanisms of current transport in bulk superconductors and in thin films in parallel and perpendicular field are also qualitatively different. For instance, in bulk samples the macroscopic current density **J** results from the gradient of the vortex density,[1] whereas for films in perpendicular field, the value of **J** is mostly determined by the curvature of flux lines.[28] By contrast, in thin films ($d \ll \lambda$) in parallel field, the current flow is not directly due to vortices, since films with $d \ll \lambda$ are almost magnetically transparent and their transport current is determined by the Meissner screening currents which flow parallel to the film surface.

The qualitative difference in physical mechanisms which control J_c for parallel and perpendicular field orientations can result in a significant angular dependence of $J_c(\varphi)$ in thin films, even without invoking the intrinsic pinning mechanism for HTS. In this paper we demonstrate this fact by presenting experimental and theoretical evidences for the strong dependence of $J_c(\varphi)$ on the orientation of **H** in LTS thin films having high crystalline isotropy, which enables one to reveal the effect of sample geometry. In our experiments we used films made of a body centered cubic Nb-47 wt % Ti solid solution. An important advantage of Nb-Ti is that the flux

pinning in Nb-Ti alloys is well understood and controllable,[3] which is not the case for most other superconducting materials. In addition, this material can easily be deposited as uniform films of controlled thickness and does not need to be grown epitaxially to be superconducting. The paper is organized as follows.

The experimental data are presented in Sec. II. The full angular dependence of $J_c(\varphi)$ at $\mathbf{H}\perp\mathbf{J}$ and its parallel ($J_{c\parallel}$) and perpendicular ($J_{c\perp}$) values have been measured for films with $d=\lambda/4$, $\lambda/2$, λ, 2λ, and 4λ, and for B ranging from 0 to 10 T. These measurements of $J_c(\varphi)$ as a function of the angle φ between $\mathbf{H}$ and the normal to the film plane show that many features of $J_c(\varphi)$ essentially depend on film thickness and that there is a marked change in behavior at about $d\approx(1-2)\lambda$. For very thin films ($d=\lambda/2$) the function $J_c(\varphi)$ exhibits sharp peaks $J_c(\varphi)\propto 1/|\varphi-90°|^{0.42}$ in the case of nearly parallel field orientation, similar to those observed for HTS films.[13–18] Extremely high values of J_c approaching 20–30 % of J_d are then observed.

In Sec. III we present a theoretical analysis of the vortex structure and critical currents in thin films ($d\ll\lambda$). An analytical solution of the London equation for the field distribution $B(x,y)$ around a single fluxon is obtained. The surface barrier H_s, the lower critical field H_{c1}, and the magnetic flux ϕ in the vortex are calculated. Reducing the film thickness significantly modifies the vortex-vortex interaction, giving rise to noncentral, position-dependent forces between vortices which decay over distances of order d, rather than λ. By means of these results, both the bulk and the surface components of $J_{c\parallel}(d)$ are evaluated. As d decreases, the bulk component of $J_{c\parallel}(d)$ is shown to increase as $1/d^2$ due to a "softening" of the vortex structure caused by the decrease of the range of the intervortex repulsion. Thereby, vortices become more strongly pinned owing to a better matching to the pinning potential, which results in a crossover between the collective and single-vortex pinning regimes below a critical thickness, d_c. At the same time, the surface magnetic pinning gives rise to a $1/d$ dependence of $J_{c\parallel}(d)$ which is in agreement with our experimental data. This mechanism gives the main contribution to J_c for our Nb-Ti films and results in a significant increase in $J_{c\parallel}$ at $d<\lambda$, with J_c being of order J_d at low fields.

Section IV is devoted to the wider implications of this analysis for the interpretation of experimental results on thin HTS films.

II. ORIENTATIONAL DEPENDENCE OF $J_c(\varphi)$ IN Nb-47% Ti FILMS

A. Experimental details

The films were fabricated by dc magnetron sputtering onto glass substrates held at room temperature using a Nb-47 wt% Ti target in an Ar plasma. The film thicknesses d were controlled by adjusting the power of the magnetron and the duration of the deposition. The films were patterned by photolithography and etched with HF/HNO_3 using a 50 μm wide by 3 mm long bridge pattern. It is important to note that the films did not have α-Ti precipitates and, therefore, they exhibit only relatively weak flux pinning, as compared to optimized Nb-Ti (see, e.g., Ref. 3). The films are believed to have grown with a largely columnar grain structure, the axes of the grains being approximately normal to the film surface. No post-deposition processing was done to enhance the flux pinning, since we wanted to keep the microstructural defect density low in order to emphasize effects arising purely from changes in the film geometry. Two sets of Nb-Ti films were fabricated in two separate systems. Both systems had a residual base pressure $\sim 10^{-7}$ Torr and evidently contributed some O (or N) to the growing films, depressing T_c below the value of 9 K expected for bulk material. Two films were fabricated in system A. These set A films had thicknesses of $\lambda/2$ (120 nm) and 1 μm (4λ). Their resistive T_c values were 8.19 K and 8.45 K, respectively, and their transitions were very sharp ($\Delta T_c/T_c<0.005$). Since the T_c values were similar, we used the set A films to study the orientational and field dependence of J_c.

Five films were fabricated in system B. They had thicknesses of 60 nm ($\lambda/4$), 120 nm ($\lambda/2$), 250 nm (λ), 500 nm (2λ), and 1 μm (4λ). The T_c values of these films were 5.39 K ($\lambda/4$), 6.54 K ($\lambda/2$), 7.34 K (λ), 8.55 K (2λ), and 8.74 K (4λ), respectively. The set B films were primarily used for studying the field and thickness dependence of $J_{c\perp}$ and $J_{c\parallel}$.

The critical currents of the two film sets were measured by means of two different techniques, both of which permitted rotation of the film plane with respect to the magnetic field $\mathbf{H}$ which was always perpendicular to the transport current density $\mathbf{J}$. In the system used for the set A films, the angular precision was 0.036° and the maximum field was 8 T. For the set B, the angular precision was 0.015° and the maximum field was 10 T. For current and voltage contacts we used indium pressure contacts with resistance less than 0.5 Ω. The critical currents I_c were determined by a standard four-probe method using a 1 μV/cm voltage criterion, and the J_c values were calculated as I_c/A, where A is the cross-sectional area of the bridge. In all cases, the dimensions of the bridge were determined by using an Alpha-Step 200 profilometer.

B. Results

Figure 1 compares the orientational dependence of J_c (φ, 1T, 4.2 K) for the set A films over the range $-10°<\varphi<100°$, where $\varphi=0°$ represents $\mathbf{H}$ perpendicular to the film plane ($J_{c\perp}$) and $\varphi=90°$ represents $\mathbf{H}$ parallel to the film plane ($J_{c\parallel}$). In general, both films exhibit a sharp peak in parallel field and J_c falls to a minimum before rising to a much smaller peak which is nominally in the vicinity of $\varphi=0°$ ($H_\perp$). However, there are important differences between the curves. First, the $J_c(\varphi)$ values of the $\lambda/2$ film were 3–20 times greater than the $J_c(\varphi)$ values of the 4λ films. Second, the peak in $J_c(\varphi)$ in parallel field was much sharper in the case of the $\lambda/2$ film and was cusp-shaped, as shown in Fig. 2. Additionally, the angular dependence of $J_c(\varphi)$ for the $\lambda/2$ film in the vicin-

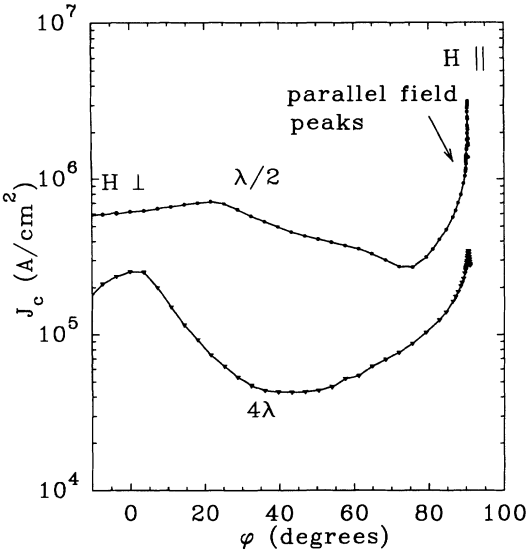

FIG. 1. The orientational dependence of $J_c(\varphi)$ for the $\lambda/2$ and 4λ set A films.

ity of the cusp can be well described by the power law $J_c(\varphi) \propto 1/|\varphi - 90°|^{0.423}$, as shown in the inset to Fig. 2. In the case of the 4λ film, $J_c(\varphi)$ has a more shallow rounded peak at $\varphi \approx 90°$ which did not obey any power law for its orientational dependence. Third, the nominally perpendicular peak was larger for the 4λ film than for the $\lambda/2$ film. Also, this peak was located at $\varphi = 5°$ for the 4λ films but at $\varphi = 21°$ for the $\lambda/2$ film.

Figure 3 plots $J_{c\perp}$ and $J_{c\parallel}$ values obtained over the range 0–8 T at 4.2 K for both films. The highest values of J_c are obtained for the $\lambda/2$ film with $H_\parallel$ and the lowest for the 4λ film with $H_\parallel$. By contrast, $J_{c\perp}$ is greater

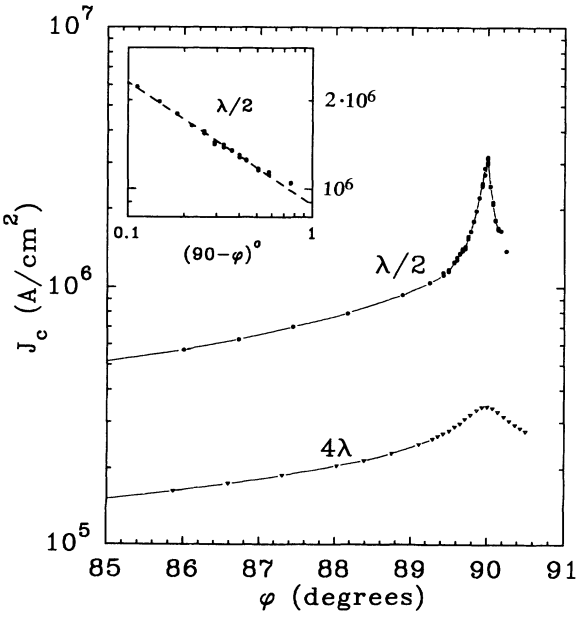

FIG. 2. The angular structure of the peak in $J_c(\varphi)$ in nearly parallel field for the $\lambda/2$ set A film. Inset shows the fit of the data to the $1/|\varphi - 90°|^{0.423}$ dependence (dashed line).

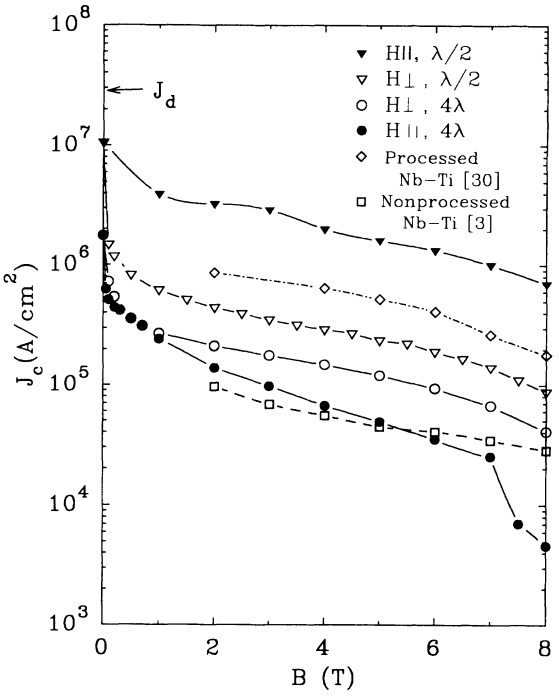

FIG. 3. Field dependencies of J_c for the $\lambda/2$ and 4λ set A films for parallel and perpendicular orientations.

for the 4λ than for the $\lambda/2$ film. Thus the anisotropy of $J_c(\varphi)$ for the $\lambda/2$ film is not only much higher but the ratio $J_{c\parallel}/J_{c\perp}$ is of order 20 for the $\lambda/2$ film but of order $\frac{1}{3}$ for the 4λ film. The magnitudes of J_c also display important features. In the zero-field limit J_c reaches $\sim 1\times 10^7$ A/cm^2 and $\sim 1.8\times 10^6$ A/cm^2 for $\lambda/2$ and 4λ films, respectively. The value of J_c for the $\lambda/2$ film is about 30% of the depairing current density J_d for the bulk Nb-47 wt % Ti which can be calculated from Eq. (1) as follows,

$$J_d = 0.544 H_c/\lambda \approx 3\times 10^7 \text{ A/cm}^2$$

(we took $\mu_0 H_c = 0.20$ T and $\lambda = 250$ nm).

At 5 T, a common reference point for Nb-Ti, the $\lambda/2$ film had J_c values at 1.8×10^6 A/cm^2 for $H_\parallel$ and 2.5×10^5 A/cm^2 for $H_\perp$, while the 4λ film had J_c values of 1×10^5 A/cm^2 for $H_\perp$ and 5×10^4 A/cm^2 for $H_\parallel$. For comparison we plot the data of Cooley *et al.*,[30] for the most optimized bulk sample yet made ($J_c \sim 5.3\times 10^5$ A/cm^2 at 4.2 K, 5 T) and the data for a precipitate-free bulk sample of Nb-47 wt % Ti for which $J_c \sim 4\times 10^4$ A/cm^2 at 5 T, 4.2 K (see, e.g., Ref. 3). Thus at one extreme a thin film ($\lambda/2$) exhibits a $J_{c\parallel}$ values which are about 3 times higher than the most optimized two-phase Nb-Ti sample ever made, even though it contains no flux-pinning α-Ti precipitates. At the other extreme, for both $\lambda/2$ and 4λ films, $J_{c\perp}$ is much lower, and the $J_{c\parallel}$ for the 4λ film is comparable to the precipitate-free bulk material.

The field dependence of $J_{c\parallel}$ and $J_{c\perp}$ for the set B films is shown in Fig. 4. A systematic transition in the relative magnitudes of $J_{c\parallel}(H)$ to $J_{c\perp}(H)$ is seen in the films. The ratio $(J_{c\parallel}/J_{c\perp})$ is of order 30 for the $\lambda/4$ film, decreases as

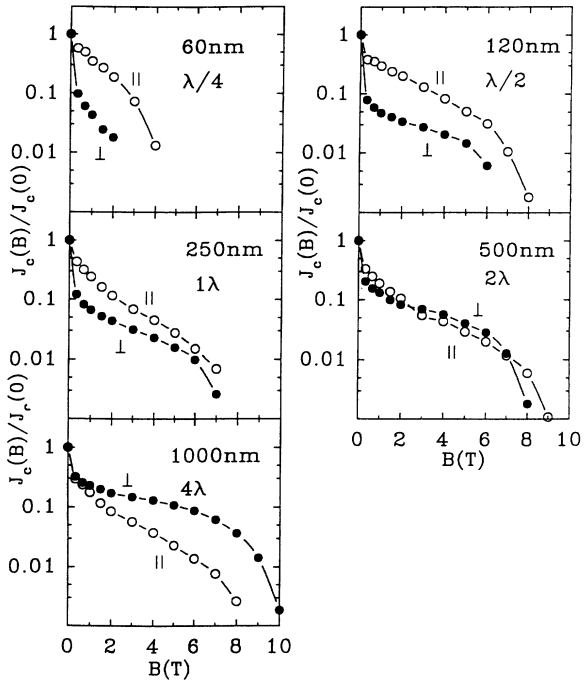

FIG. 4. Field dependencies of $J_{c\parallel}$ for the set B films of different thicknesses.

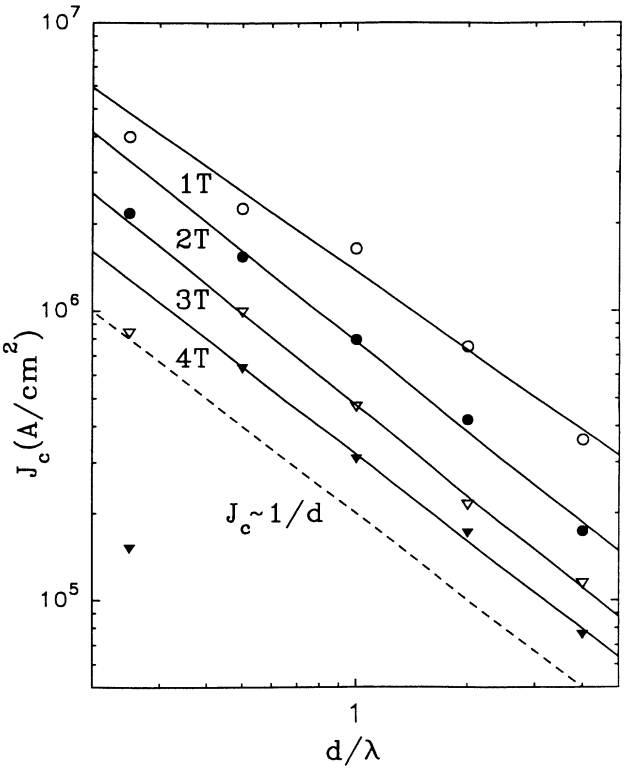

FIG. 5. Thickness dependencies of $J_{c\parallel}$ at different B extracted from the data of Fig. 4. The dashed line corresponds to the $1/d$ dependence.

d increases and is of order $\frac{1}{3}$ for the 4λ film. In this regard, the set B films exhibit similar field dependences to the set A films.

In Fig. 5, we plot the $J_{c\parallel}$ values at 1, 2, 3, and 4 T for each set B films as a function of d, where the solid lines are linear regression fits to the $J_{c\parallel}$ data. We find that, the thickness dependence of $J_{c\parallel}$ is approximately inversely proportional to d, as seen by comparing our results to a $1/d$ line. At the same time, one should keep in mind that the data shown in Fig. 5 give only a qualitative tendency of the $J_{c\parallel}(d)$ dependence, since the set B films of different thicknesses had different T_c values. For this reason the data for the $\lambda/4$ film at 3 and 4 T were excluded from the regression, since these fields were close to H_{c2}.

III. VORTICES IN THIN FILMS

A. Field distribution in a single vortex

In this section we consider a single vortex in a thin film, assuming that both the external magnetic field $\mathbf{H}$ and the vortex are parallel to the film surface. The film thickness d is assumed to be much larger than the coherence length ξ, which enables one to describe the field distribution $B(x,y)$ within the framework of the London equation

$$\lambda^2\nabla^2 B - B = -\phi_0\delta(\mathbf{r}-\mathbf{r}_0) , \tag{2}$$

where $\mathbf{r}_0$ is the coordinate of the vortex core, and the axes x and y are perpendicular and parallel to the film surface, respectively. The boundary conditions to Eq. (2) are that the normal component of the current density $\mathbf{J}=(c/4\pi)\mathrm{curl}\mathbf{B}$ vanishes at the film surface ($x=\pm d/2$). A standard way to satisfy this boundary condition is to consider a periodic chain of vortex-antivortex "images" in an infinite sample (see, e.g., Refs. 31–35). This reduces the case of the film geometry to the well-known description of vortices in an infinite superconductor, where the fluxon characteristics can be expressed in terms of an infinite series of modified Bessel functions $K_0(nd/2\lambda)$, $n=1,2,3,\ldots$.

In this paper we employ another approach,[31] which enables one to obtain an analytic single-vortex solution of Eq. (2) at $d \ll \lambda$. Since the film is assumed to be infinite along the y axis, it is convenient to make a Fourier transformation of $B(x,y)$ in y, which turns Eq. (2) into the following ordinary differential equation for the mixed Fourier component $B_k(x)$,

$$\lambda^2 B_k'' - (1+\lambda^2 k^2)B_k = -\phi_0 e^{-iky_0}\delta(x-x_0) . \tag{3}$$

Here the prime denotes the derivative over x, and

$$B_k(x) = \int_{-\infty}^{\infty} \exp(-iky)B(x,y)dy . \tag{4}$$

In this representation the boundary condition $J_x(\pm d/2)=0$ reduces to $B_k(\pm d/2)=0$, and the delta function in Eq. (3) gives rise to a discontinuity of $B_k'(x)$ at $x=x_0$. Indeed, by integrating Eq. (3) from $x=x_0-0$ to x_0+0, and using the continuity of $B_k(x)$ at $x=x_0$, we obtain

$$\lambda^2[B_k'(x_0+0)-B_k'(x_0-0)] = -\phi_0\exp(-iky_0) . \tag{5}$$

The solution of Eq. (3) which satisfies these boundary

conditions has the form

$$B_k(x)=\frac{\phi_0 e^{-iky_0}}{2\lambda^2 p\,\sinh pd}[\cosh p(d-|x-x_0|) -\cosh p(x+x_0)] , \quad (6)$$

where $p=(k^2+1/\lambda^2)^{1/2}$. For thick ($d\gg\lambda$) films, one can put $dp\to\infty$ everywhere, except for a narrow layer of thickness $\sim\lambda$ at the surface (see below). Then the inverse Fourier transformation of Eq. (6) (see, e.g., Ref. 36) yields $B(\mathbf{r})$ in the Abrikosov fluxon[29]

$$B(x,y)=\frac{\phi_0}{2\pi\lambda^2}K_0\left[\frac{|\mathbf{r}-\mathbf{r}_0|}{\lambda}\right] \quad (7)$$

for which $B(\mathbf{r})$ decays over the penetration depth λ. In this paper we focus on the opposite limiting case of thin films ($d\ll\lambda$) for which $B(\mathbf{r})$ in the vortex decays over a length $\sim d$ which is much shorter than λ. In this case the main contribution to $B(\mathbf{r})$ comes from the Fourier components $B_k(x)$ with wave vectors k much larger than $1/\lambda$, for which one can set $p=|k|$. As a result, the inverse Fourier transformation of Eq. (6) can be performed exactly (details are given in Appendix), leading to the following field distribution $B(x,y)$ in the fluxon

$$B(x,y)=\frac{\phi_0}{4\pi\lambda^2}\ln\frac{\cosh\frac{\pi}{d}(y-y_0)+\cos\frac{\pi}{d}(x+x_0)}{\cosh\frac{\pi}{d}(y-y_0)-\cos\frac{\pi}{d}(x-x_0)} \quad (8)$$

for which both $B(x,y)$ and the normal component of $\mathbf{J}(x,y)$ vanish at the film surface [$B(\pm d/2,y)=0$ and $J_x(\pm d/2,y)=0$]. The function given by Eq. (8) is a solution of the Laplace equation $\lambda^2\nabla^2 B=-\phi_0\delta(\mathbf{r}-\mathbf{r}_0)$ which reduces to the London equation Eq. (2) if one neglects the second term in the left-hand side of Eq. (2) responsible for the London screening. This is a specific feature of thin films with $d\ll\lambda$, for which the London screening is negligible and gives only a small correction to Eq. (8) of order $d^2/\lambda^2\ll 1$ (see Appendix), since the film with $d\ll\lambda$ is almost magnetically transparent.

The field distribution given by Eq. (8) is shown in Fig. 6. As follows from Eq. (8), unlike the fluxon in the infinite sample, $B(x,y)$ in the film is anisotropic and vanishes at the film surface ($x=\pm d/2$). Another distinctive feature of the case $d\ll\lambda$ is that $B(x,y)$ in the fluxon decays exponentially along the film (y axis) over the length d/π much smaller than λ, but in the vicinity of the vortex core $B(x,y)$ turns out to be analogous to that for the infinite sample. For instance, at small distances

$$r=[(x-x_0)^2+(y-y_0)^2]^{1/2}\ll d$$

from the vortex core, Eq. (8) yields the same current density distribution $J(r)=c\phi_0/8\pi^2\lambda^2 r$ as that for the fluxon in the infinite superconductor.

Thus, the effect of the film geometry manifests itself at distances r comparable to the thickness d. As a result, the magnetic field of the fluxon is mostly localized in a domain of size $\sim d$ inside the film, the characteristic amplitude of $B(x,y)$ about the vortex core remaining of the same order of magnitude as that for the infinite sample. This situation qualitatively differs from that for the thin film in perpendicular field, where $B(x,y)$ in the fluxon decays along the surface over the length λ^2/d which is much larger than λ,[27,29] since the magnetic lines are mostly localized outside the film.

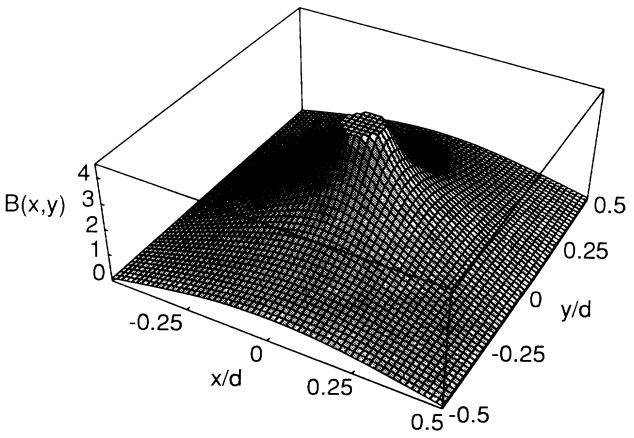

FIG. 6. Field distributions $B(x,y)$ in a fluxon calculated by means of Eq. (8) [$B(x,y)$ is measured in the units of $\phi_0/4\pi\lambda^2$].

B. Flux quantum, surface barrier, and H_{c1}

The analytical solution (8) enables one to calculate relevant characteristics of the fluxon in a thin film without analyzing a cumbersome series of Bessel functions. For instance, the above features of $B(x,y)$ give rise to a smaller magnetic flux ϕ in the vortex parallel to the film surface as compared to the flux quantum ϕ_0.[34,35] The magnitude of ϕ can be written in the form

$$\phi(x_0)=\int_{-d/2}^{d/2}B_0(x,x_0)dx , \quad (9)$$

where $B_0(x)$ is given by Eq. (6) with $k=0$ and $p=1/\lambda$. Then a simple integration of Eq. (9) yields[34]

$$\phi(x_0)=\phi_0\left[1-\frac{\cosh x_0/\lambda}{\cosh d/2\lambda}\right] . \quad (10)$$

Therefore, for thick films ($d\gg\lambda$) the flux $\phi(x_0)$ equals ϕ_0 everywhere, except for a surface layer, where $\phi(l)$ changes over the distance $l=d/2-x_0$ from the surface as follows

$$\phi(l)=\phi_0[1-\exp(-l/\lambda)] . \quad (11)$$

In the opposite case of very thin films ($d\ll\lambda$), formula (10) reduces to

$$\phi(x_0)=\frac{\phi_0 d^2}{8\lambda^2}\left[1-\frac{4x_0^2}{d^2}\right] . \quad (12)$$

The flux $\phi(x_0)$ is then a maximum in the center, $\phi(0)=\phi_0 d^2/8\lambda^2$ and vanishes at the film surface ($x_0=\pm d/2$). Here $\phi(0)$ is much less than ϕ_0, since the magnetic field in the vortex is mostly localized in a domain of area $\sim d^2$, unlike the fluxon in the infinite sample for which this area is of order λ^2.

To calculate the lower critical field H_{c1} and the surface barrier for flux penetration, we consider the part of the

thermodynamic potential G associated with vortices:[34,37,38]

$$G=\frac{\phi_0}{4\pi}\sum_n \int \delta(\mathbf{r}-\mathbf{r}_n)[B_L(\mathbf{r})+\tfrac{1}{2}B_V(\mathbf{r})-H(\mathbf{r})]dx\,dy \ , \tag{13}$$

where $\mathbf{r}_n$ is the coordinate of the nth fluxon, $B_V(\mathbf{r})$ is the total field produced by the vortices, and $B_L(x)$ is the Meissner screening field which satisfies the London equation with the boundary conditions $B_L(\pm d/2)=H\mp 2\pi I/c$, where H is the external magnetic field, and I is the total transport current along the y axis. The solution of the London equation is

$$B_L(x)=H\frac{\cosh x/\lambda}{\cosh d/2\lambda}-\frac{2\pi I}{c}\frac{\sinh x/\lambda}{\sinh d/2\lambda} \ . \tag{14}$$

We first consider the potential G for a single vortex as a function of its position x_0 in the film. Then Eq. (13) takes the form

$$G_0=\phi_0[2B_L(x_0)-2H+B_V(x_0)]/8\pi \ ,$$

where B_V and B_L are given by Eqs. (8) and (14), respectively. Since the field $B_V(\mathbf{r})$ diverges logarithmically as $x\to x_0$ and $y\to y_0$, we take the standard limit $|\mathbf{r}-\mathbf{r}_0|\to\xi$ when calculating $B_V(x_0)$ in the vicinity of the vortex core. As a result, the potential $G_0(x_0)$ at $d\ll\lambda$ becomes

$$G_0(x_0)=\left[\frac{\phi_0}{4\pi\lambda}\right]^2\left[\ln\left[\frac{2d}{\pi\xi}\cos\frac{\pi x_0}{d}\right]+\beta\right] -\frac{H\phi_0 d^2}{32\pi\lambda^2}\left[1-\frac{4x_0^2}{d^2}\right]-J\frac{\phi_0 x_0}{c} \ . \tag{15}$$

The first term on the right-hand side of Eq. (15) describes the self-energy of the vortex, where the coefficient $\beta=0.38$ accounts for the core energy[39] which is the same as for the vortex in the infinite sample, since the film thickness is assumed to be much larger than the core radius ξ. The second term in Eq. (15) is the energy of the vortex in the magnetic field, $-\phi(x_0)H/4\pi$, with the flux $\phi(x_0)$ given by Eq. (12), and the last term is the work of the Lorentz force, where $J=I/d$ is the mean linear transport current density. The equilibrium vortex position in the film is determined by the condition $\partial G_0/\partial x_0=0$, whence

$$\frac{\phi_0}{4d}\tan\frac{\pi x_0}{d}=Hx_0-J\frac{4\pi\lambda^2}{c} \ . \tag{16}$$

Making use of Eqs. (15) and (16), we consider the Bean-Livingston surface barrier[40] which has been calculated for thin films in Refs. 32, 34, 41, and 42 (see also Ref. 49). Shown in Fig. 7, the energy barrier $G_0(x_0)$ displays different dependencies on x_0 in four characteristic field regions: $H<H_m$, $H_m<H<H_{c1}$, $H_{c1}<H<H_s$, and $H>H_s$. For instance, at $H>H_m$ there first appears the stable solution $x_0=0$ of Eq. (16) which corresponds to a stable vortex position in the center of the film, the field H_m being

$$H_m=\pi\phi_0/4d^2 \ . \tag{17}$$

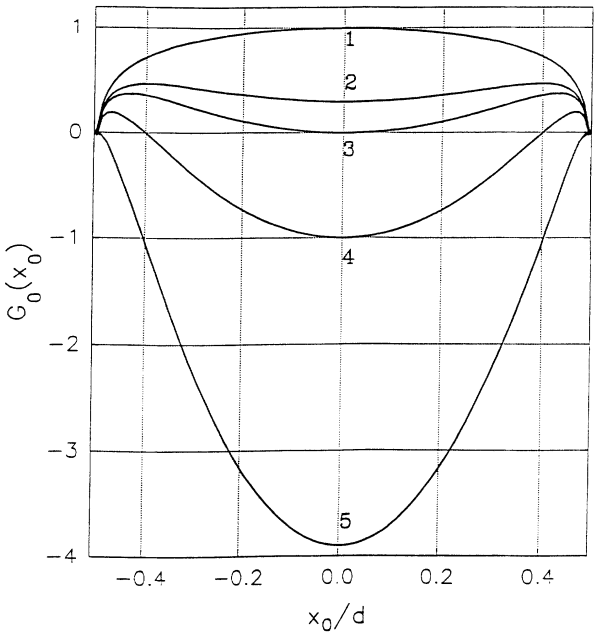

FIG. 7. Single-vortex thermodynamic potential (15) for different H at $J=0$: $H<H_m$(1), $H_m<H<H_{c1}$ (2), $H=H_{c1}$ (3), $H_{c1}<H<H_s$ (4), and $H>H_s$ (5).

At $H_m<H<H_{c1}$ there appears an exit barrier for the vortex which therefore can be trapped by the magnetic potential well shown in Fig. 7. This corresponds to a metastable state, since the potential $G_0(x_0)$ remains positive for all x_0. At $H>H_{c1}$ the value $G(0)$ becomes negative. The lower critical field H_{c1} is then determined by the condition $G(0)=0$, which yields

$$H_{c1}=\frac{2\phi_0}{\pi d^2}\left[\ln\frac{d}{\xi}+\gamma\right] \ , \tag{18}$$

where $\gamma=\ln(2/\pi)+\beta=-0.07$. For Nb-Ti films with $d=\lambda/2=120$ nm, Eq. (18) gives $H_{c1}=0.3$ T. A formula for H_{c1} for thin films was first obtained by Abrikosov[31] with a logarithmic accuracy (see also Refs. 32–35). Notice that Eq. (18) gives the same dependence of H_{c1} upon d as the results of Refs. 31, 34, and 35, except for the numerical value of γ.

At $H>H_{c1}$, vortices still have to overcome the entry barrier in $G_0(x_0)$ as long as $H<H_s$. As H increases, the maximum in $G_0(x_0)$ in Fig. 7 moves toward the film surface. At a certain H_s, the distance between the maximum in $G(x_0)$ and the point $x=d/2$ becomes of order ξ, and the surface barrier disappears. The field H_s at $J=0$ can be calculated from Eq. (16) with $x_0=d/2-\xi$, whence:[32,34]

$$H_s=\phi_0/2\pi d\xi \ . \tag{19}$$

As follows from Eqs. (18) and (19), the fields H_{c1} and H_s can be much larger in thin films than in bulk superconductors, for which

$$H_{c1}\approx(\phi_0/4\pi\lambda^2)\ln[(\lambda/\xi)+0.497]$$

(Ref. 39) and $H_s = H_c = \phi_0/2\sqrt{2}\pi\lambda\xi$, where H_c is the thermodynamic critical field.[28,29] Qualitatively, the values H_{c1} and H_s at $d \ll \lambda$ can be obtained from the bulk H_{c1} and H_s by the replacement of the London penetration depth λ by the length d/π over which the magnetic field varies along the film.

At $J > 0$ the function $G_0(x_0)$ is asymmetric, due to the self-field effects. Above the critical value J_c, Eq. (16) has no stable solutions, since the self-field becomes comparable to H_s and the magnetic potential well shown in Fig. 7 disappears. The value of J_c above which the minimum in $G_0(x_0)$ disappears is determined by the set of equations $\partial G_0(x_0, J_c)/\partial x_0 = 0$ and $\partial^2 G_0(x_0, J_c)/\partial x_0^2 = 0$, where G_0 is given by Eq. (15). The first equation reduces to Eq. (16), and the second one yields $x_0 = (d/\pi)\cos^{-1}(H_m/H)^{1/2}$. Substituting this value of x_0 into Eq. (16), one obtains[32,34]

$$J_c = \frac{c\,dH}{4\pi^2\lambda^2}\left\{\cos^{-1}\left[\frac{H_m}{H}\right]^{1/2} - \left[\frac{H_m}{H}\left[1-\frac{H_m}{H}\right]\right]^{1/2}\right\}. \tag{20}$$

This formula, which determines the critical current density at $H \approx H_{c1}$ due to the surface magnetic pinning, will be discussed in the next section in more detail. Here we just notice that $J_c(H)$ given by Eq. (20) increases with H due to the increase of the depth of magnetic potential well $G_0(x_0)$ with H (see Fig. 7).

C. Vortex-vortex interactions in thin films

In the presence of an external magnetic field $H > H_{c1}$, a vortex interacts with both the screening Meissner field and other fluxons. As follows from Eq. (15), the force $f = -\partial G/\partial x_0$ produced by the screening current $J_L = -(c/4\pi)\partial B_L/\partial x_0$ is given by the standard formula for the Lorentz force:

$$f = \frac{\phi_0}{c} J_L \tag{21}$$

regardless of the film thickness d.[32,34]

By contrast, the magnetic interaction between vortices is strongly affected by the film geometry for $d \ll \lambda$ due to the reduced magnitude of the flux quantum $\phi(x_0)$. Making use of Eqs. (13), we can write the thermodynamic potential G of any vortex configuration in the form

$$G = \sum_n G_0(\mathbf{r}_n) + \frac{1}{2}\sum_{n\neq m} U(\mathbf{r}_n, \mathbf{r}_m), \tag{22}$$

where $G_0(\mathbf{r}_n)$ is the thermodynamic potential Eq. (15) of a single vortex located at $\mathbf{r} = \mathbf{r}_n$, and

$$U(\mathbf{r}_n, \mathbf{r}_m) = \phi_0 B_v(\mathbf{r}_n, \mathbf{r}_m)/4\pi$$

is the energy of the pair vortex interaction. Here $B_V(\mathbf{r}_n, \mathbf{r}_m)$ is the field at the point $\mathbf{r}_m$ caused by the vortex being at the point $\mathbf{r}_n$ [as follows from Eq. (8), the field B_V is symmetric, i.e., $B(r_n, r_m) = B(r_m, r_n)$]. Using Eq. (8), one obtains

$$U(\mathbf{r}_n, \mathbf{r}_m) = \left[\frac{\phi_0}{4\pi\lambda}\right]^2 \ln\frac{\cosh\frac{\pi}{d}(y_n - y_m) + \cos\frac{\pi}{d}(x_n + x_m)}{\cosh\frac{\pi}{d}(y_n - y_m) - \cos\frac{\pi}{d}(x_n - x_m)}. \tag{23}$$

Unlike the infinite superconductor, the function $U(\mathbf{r}_n, \mathbf{r}_m)$ depends not only on the spacing between vortices $r_{nm} = |\mathbf{r}_n - \mathbf{r}_m|$, but on their positions in the film as well. For instance, if a vortex is at the surface ($x_n = d/2$), it has zero magnetic flux $\phi(x_n)$ and therefore does not interact with other vortices. In addition, the potential $U(\mathbf{r}_n, \mathbf{r}_m)$ of the pair vortex interaction in thin films changes over the length d, which can be much shorter than λ.

As an illustration, we consider the force $\mathbf{f}$ between two vortices at the points $x_n = x_0$, $y_n = y_0$, and $x_m = -x_0$, $y_m = -y_0$ (Fig. 8). The corresponding field and current distributions determined by Eq. (8) are shown in Fig. 9. For such a symmetric case, the differentiation of Eq. (23) gives the components of the force, $2f_x = -\partial U/\partial x_0$ and $2f_y = -\partial U/\partial y_0$ in the form

$$f_x = \frac{\phi_0^2}{16\pi\lambda^2 d}\frac{\sin\frac{2\pi x_0}{d}}{\cosh\frac{2\pi y_0}{d} - \cos\frac{2\pi x_0}{d}}, \tag{24}$$

$$f_y = \frac{\phi_0^2}{8\pi\lambda^2 d}\frac{\tanh\frac{\pi y_0}{d}\cos^2\frac{\pi x_0}{d}}{\cosh\frac{2\pi y_0}{d} - \cos\frac{2\pi x_0}{d}}, \tag{25}$$

where $0 < x_0 < d/2$, $0 < y_0 < \infty$. Both components f_x and f_y are positive, which corresponds to a vortex repulsion at any x_0 and y_0. However, unlike the infinite superconductor, the force $\mathbf{f}$ generally is not central, that is, the vector $\mathbf{f}$ is not parallel to the line which connects the fluxons (see Figs. 8 and 9). A similar situation occurs in anisotropic superconductors.[45–47]

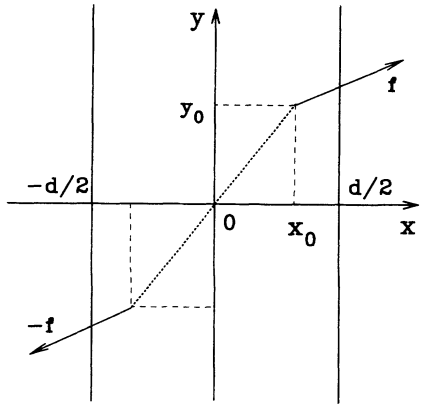

FIG. 8. Noncentral forces between two vortices being at $x = \pm x_0$ and $y = \pm y_0$.

Formulas (24) and (25) simplify if the vortices are on the film axis ($x_0=0$). Then

$$f_x=0, \quad f_y=\frac{\phi_0^2}{8\pi\lambda^2 d\sinh(2\pi y_0/d)} . \tag{26}$$

Likewise, for the vortices lying on a line perpendicular to the film axis ($y_0=0$):

$$f_y=0, \quad f_x=\frac{\phi_0^2}{16\pi\lambda^2 d}\cot\frac{\pi x_0}{d} . \tag{27}$$

At small distances between vortices ($x_0^2+y_0^2\ll d^2$), the forces f_x and f_y given by Eqs. (24) and (25) do not depend on d and are the same as for the infinite sample. However, as y_0 increases, the force **f** exponentially decreases over the length $d/\pi\ll\lambda$. On the other hand, for fixed y_0 and changing x_0, the force **f** decreases as x_0 increases, vanishing at $x_0=d/2$. The latter is due to the zero magnetic flux $\phi(x_0)$ for vortices being at the film surface [see Eqs. (10)–(12)].

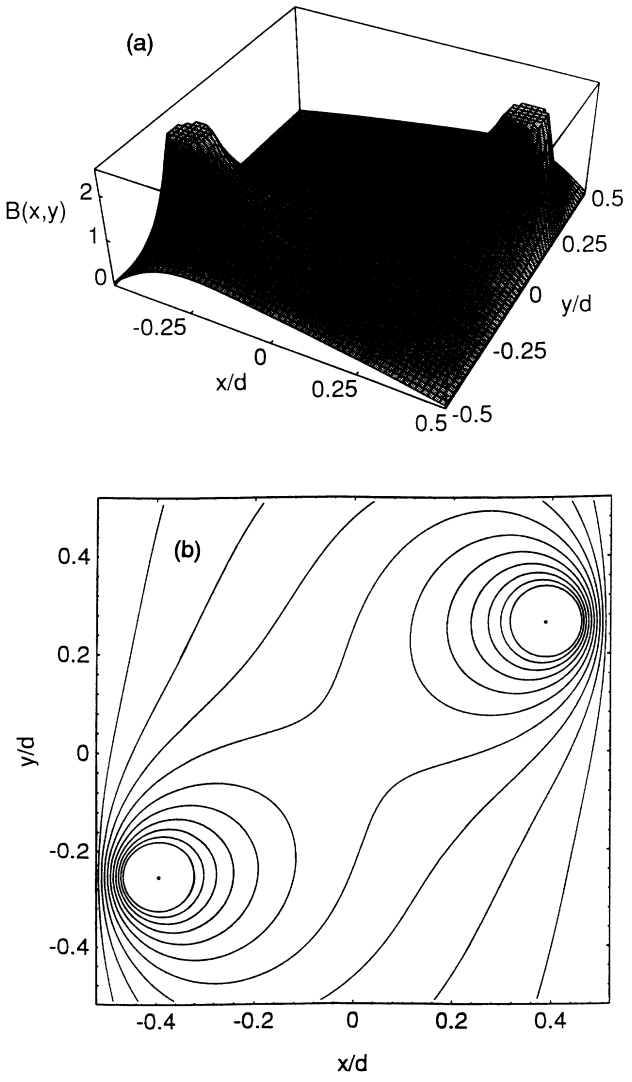

FIG. 9. Field distribution (a) and current lines (b) of a pair of fluxons located at $x_0=\pm0.4d$ and $y_0=\pm0.25d$ calculated by means of Eq. (8) [$B(x,y)$ is measured in the units of $\phi_0/4\pi\lambda^2$].

IV. CRITICAL CURRENTS OF THIN FILMS

A. Bulk pinning

In the Meissner state at $H<H_{c1}$ (or H_s) vortices are absent and the critical current density J_c is determined by the screening field described by Eq. (14). Assuming that J_c is achieved when the maximum current density $J(x)$ at the film surface reaches J_d, we obtain from Eq. (14) that at $d\ll\lambda$ the value J_c is given by

$$J_c=\left[1-\frac{H}{H_f}\right]J_d , \tag{28}$$

where

$$H_f=\frac{8\pi\lambda^2 J_d}{cd}=\frac{2\phi_0}{3\sqrt{3}\pi\xi d} . \tag{29}$$

Here $J_c(H)$ linearly decreases with increasing H, the field H_f being of the order of H_s. Since at $d\ll\lambda$, both H_{c1} and H_s increase as d decreases, the field range over which J_c is determined by the Meissner currents turns out to be much wider than for $d\gg\lambda$.

At $H>H_{c1}$ (or H_s, depending on the degree of the surface roughness), vortices can penetrate the film, and J_c is then determined by the balance of the Lorentz and pinning forces. Here we focus on the case of thin films with $d\ll\lambda$ in parallel field, for which the transport current I is mostly due to the Meissner component J_L, unlike bulk superconductors, where I is determined by the gradient of the fluxon density. In both cases, however, the Lorentz force is given by the same formula (21), where J_L is a mean transport current density. As follows from Eq. (21), the Lorentz force is independent of the film thickness. Thus we now consider the dependence of pinning forces on film thickness.

Unlike a bulk sample or a thin film in perpendicular field, where vortices form a triangular lattice in the absence of pinning, the vortex structure in thin films in parallel field can be more complicated, due to the noncentral, position-dependent interaction between vortices described above. In addition, the vortices are in a nonuniform external potential caused by the screening field $B_L(x)$ (see Fig. 7). As a result, the vortex structure is generally nonuniform across the film and nonperiodic along the film, even in the absence of bulk pinning. For instance, at $H\approx H_{c1}$ vortices form a single periodic chain along the film axis;[31–34] however, the further increase of H leads to the successive splitting of the initial chain[32,43,44] and the appearance of additional vortex rows. Here we confine ourselves to a qualitative analysis of J_c at $H_{c1}\ll H\ll H_{c2}$, assuming that the elementary pinning potential $U_p(\mathbf{r})$ is the same as in the bulk sample.

Now we estimate a mean equilibrium vortex density $n(H)$ in the film in the high field limit $H\gg H_{c1}$, where the number of vortex rows is much more than unity. The value $n(H)$ is determined by a competition between the

intervortex repulsion and the gain in the magnetic energy $-\phi nH/4\pi$. Here the mean energy of vortex interaction per unit length of a fluxon is of order $d^2n(\phi_0/4\pi\lambda)^2$, where d^2n is a number of vortices within the effective range $\sim d$ of the fluxon interaction [see, Eq. (22)]. Since the mean flux quantum ϕ in thin films is of order $\phi_0 d^2/12\lambda^2$, we find that

$$G \sim d^2 n^2 \left[\frac{\phi_0}{48\pi\lambda} \right]^2 - \frac{\phi_0 d^2}{48\pi\lambda^2} nH \ . \tag{30}$$

Minimization of this expression with respect to n gives a thickness-independent fluxon density $n \sim H/\phi_0$ which is of the order of that for bulk superconductors. This qualitative estimation is in agreement with previous calculations of the vortex structure in thin films,[32,33] which have shown that vortices at $H \gg H_{c1}$ form the same triangular lattice as that in the infinite superconductor provided that all vortex rows have the same period along the film. The latter condition is rather an *a priori* assumption, nevertheless we shall use the fact that $n \sim H/\phi_0$ for further qualitative analysis for which knowledge of the detailed structure of the mixed state is not critical.

Since the Nb-Ti from which our films were fabricated seems to exhibit only a weak bulk pinning, we estimate J_c by means of a collective pinning model[2] in which J_c is given by

$$J_c \sim \frac{c}{H} \left[\frac{W}{V_c} \right] , \tag{31}$$

where $W = n_p f_p^2$, f_p is an averaged elementary pinning force, and n_p is the density of pinning centers. The correlation volume $V_c = R_c^2 L_c$ is determined by the competition between elastic and pinning energies, the longitudinal (L_c) and transverse (R_c) correlation lengths being[2]

$$R_c \sim \frac{8\pi r_p^2}{W} c_{44}^{1/2} c_{66}^{3/2} \ , \tag{32}$$

$$L_c \sim R_c \sqrt{c_{44}/c_{66}} \ , \tag{33}$$

where c_{66} and c_{44} are the shear and tilt elastic moduli of the vortex structure, respectively. We consider here the 3D core pinning for which $R_c < d$, and characteristic pin sizes, r_p, are of order ξ. At $H_{c1} \ll H \ll H_{c2}$, both the tilt (c_{44}) and the bulk (c_{11}) moduli are of the order of the mean interaction energy of fluxons per unit volume, $\langle U \rangle n^2$.[48] However, as follows from Eq. (23), the value $\langle U \rangle$ for $d \ll \lambda$ is strongly reduced by the factor d^2/λ^2, as compared to the case $d \gg \lambda$ because of the decrease of the effective range of the intervortex repulsion. Hence, it follows that

$$c_{11}^{(f)} \sim \frac{d^2}{\lambda^2} c_{11}^{(b)}, \quad c_{44}^{(f)} \sim \frac{d^2}{\lambda^2} c_{44}^{(b)} \ , \tag{34}$$

where the indices b and f concern the cases $d \gg \lambda$ and $d \ll \lambda$, respectively. Formulas (34) also follow from the expressions for nonlocal elastic moduli,

$$c_{44}(k) = c_{44}(0)/(1+\lambda^2 k^2)$$

and

$$c_{11}(k) = c_{11}(0)/(1+\lambda^2 k^2)$$

derived by Brandt[48] for the bulk case $d \gg \lambda$. These formulas do reduce to Eq. (34), if one takes into account the fact that for thin films with $d \ll \lambda$, the minimum characteristic wave vector k of elastic distortion of vortex structure is of order π/d.

By contrast, the shear modulus c_{66} is not dispersive, as long as $ka \ll 1$, where $a \sim (\phi_0/H)^{1/2}$ is the spacing between vortices.[48] Hence it follows that for $H_{c1} \ll H \ll H_{c2}$

$$c_{66}^{(f)} \sim c_{66}^{(b)} \ . \tag{35}$$

This formula reflects the fact that the shear of neighboring vortex rows at $H_{c1} \ll H \ll H_{c2}$ is determined by the short-range part of the fluxon interaction $U(\mathbf{r})$ on lengths of the order of the mean distance between vortices $a \ll d$, unlike the tilt and compression of the vortex structure for which the whole interaction range $r < d$ is essential. Since, however, the vortex spacing $a \sim (\phi_0/H)^{1/2}$ and the characteristic interaction energy $U(a)$ at $a \ll d$ are of the same order of magnitude for both thin films and infinite samples, we again arrive at Eq. (35).

Making use of Eqs. (31)–(35), we can now evaluate the dependence of J_c on film thickness d in the regime of 3D bulk pinning (for which $R_c \ll d$), assuming that the elementary pinning forces f_p are independent of d, and that the main effect results from the dependence of c_{44} on d. Then we obtain that $R_c \propto c_{44}^{1/2} c_{66}^{3/2} \propto d$, $L_c \sim R_c c_{44}^{1/2}/c_{66}^{1/2} \propto d^2$, whence $V_c = R_c^2 L_c \propto d^4$, and

$$J_c^{(f)} \simeq \frac{cW^2}{(8\pi r_p^2)^{3/2} c_{44} c_{66}^2 H} \sim \frac{\lambda^2}{d^2} J_c^{(b)} \ . \tag{36}$$

Therefore $J_c(d)$ increases as d decreases, which gives rise to a crossover between collective and single-vortex pinning regimes below a critical thickness d_c. Indeed, the elastic moduli c_{11} and c_{44} in thin films decrease as the thickness d decreases. Such a "softening" of the vortex structure leads to a better matching of fluxons to pinning centers, which results in a corresponding increase of $J_c(d)$ and a drop in R_c and L_c as d decreases. As R_c becomes comparable to a, the vortex lattice becomes highly deformed and its continuum elastic description is no longer valid. In the limiting case $R_c < a$ the correlation volume contains only one vortex, which implies that each fluxon is virtually pinned independently and, instead of the collective pinning, there arises a single-vortex pinning. Similar crossover between the single-vortex and collective regimes of pinning in bulk superconductors can occur under changing T and B.[2,50,51] By contrast, in our case the control parameter is the film thickness; the single-vortex pinning regime occurs for $R_c(d) < a$. As follows from Eqs. (30)–(34), the condition $R_c(d) < a$ is equivalent to $d < d_c$, where the critical thickness d_c, below which the single-vortex regime arises, is given by

$$d_c \sim 64 \frac{\sqrt{8}\pi^{7/2} W \lambda^4}{H^3 r_p^2 \phi_0} \simeq 35\lambda^2 \left[\frac{J_c^{(b)}}{cHr_p} \right]^{1/2} . \tag{37}$$

When deriving Eq. (37) we used the following estimation $c_{66} \sim H\phi_0/64\pi^2\lambda^2$ (Ref. 46) and $c_{44} \sim (d/\pi\lambda)^2 H^2/8\pi$ at $H_{c1} \ll H \ll H_{c2}$. To estimate the critical thickness, d_c, we take $B_c^{(b)}=0.2$ T, $\lambda=240$ nm, $r_p=6$ nm$\simeq\xi$, $J_d=3\times10^7$ A/cm^2, and the bulk critical current density $J_c^{(b)}=7\times10^4$ A/cm^2 at $B=5$ T, which corresponds to a inoptimized Nb-47% Ti without α-Ti precipitates.[3] Then formula (37) gives $d_c \simeq 0.4\lambda$.

Therefore, the bulk component of $J_{c\parallel}(d)$ increases as d decreases, approaching the single-vortex limit at $d < d_c$. This is due to the decrease of the range of intervortex repulsion and the better matching of fluxons to pinning centers which can then occur. Notice that in the 3D collective regime, $J_{c\parallel}$ proves to be proportional to the parameter $(W/d)^2$ which depends on both the pinning strength and the film thickness. By contrast, in the single-vortex regime ($d < d_c$), the critical current density is independent of d and becomes proportional to $W^{1/3}$.[2,50] However, despite the increase of $J_{c\parallel}(d)$ in the single-vortex mode, the $J_{c\parallel}$ value still remains much smaller than J_d in the case of weak bulk pinning.[50] In order to get $J_c \sim J_d$ due to the core pinning, one has to assume the existence of a very dense ($n_p \sim 1/\xi^3$) structure of pins having sizes r_p of order ξ.[5] In this case both the discreteness and the plastic deformation of the vortex structure become essential, and J_c is determined by the direct summation of elementary pinning forces over all vortices.[2] Thus the bulk pinning seems to be too weak to account for the observed high values of $J_{c\parallel} \approx 0.2-0.3J_d$ in our $\lambda/2$ films. This is due to the fact that the films were fabricated from inoptimized Nb-Ti for which J_c even at low H is about 2–3 orders of magnitude lower than J_d (Ref. 3) (see also Fig. 3).

It is interesting to compare the above $J_{c\parallel}$ in parallel field to $J_{c\perp}$ in perpendicular field obtained in the 2D collective pinning regime ($d \ll L_c$). In this case[25]

$$J_{c\perp} = \frac{W \ln^{1/2}(2/aR_c)}{dr_p c_{66}\sqrt{8\pi}} , \tag{38}$$

where R_c is the 2D pinning correlation length determined by the equation

$$R_c = r_p c_{66}[8\pi d/W \ln(2/aR_c)]^{1/2} .$$

Hence it follows that $J_{c\perp}(d)$ exhibits a qualitatively different behavior from that of $J_{c\parallel}(d)$. For instance, $J_{c\perp}$ has a $1/d$ dependence and remains proportional to the pinning strength parameter W, even at small d. By contrast, $J_{c\parallel}$ at $d > d_c$ is proportional to W^2 [see Eq. (37)] and increases as $1/d^2$, approaching the single-vortex limit for which $J_c \propto W^{1/3}$ at $d < d_c$. Further decrease of d leads to the change of critical current control mechanism which is now determined by the Meissner currents in the absence of vortices. In this case $J_c \simeq J_d$ [see Eqs. (28) and (29)].

B. Surface pinning

In addition to the bulk component of I_c, there are also important surface contributions to I_c which can be divided into two groups. The first one is due to the change of the elementary pinning potential $U_p(\mathbf{r})$ at the surface due to variations of the density of pinning centers across the film, additional surface defects, for example, pyramidal dislocation structures,[21,22] etc. We do not discuss here those extrinsic contributions to I_c and focus instead on the intrinsic surface component of I_c which results only from the effect of the film geometry.

One of the pinning mechanisms discussed by Shmidt,[32] Clem,[42] and Takacs[44] results from the magnetic interaction of vortices with the surface. Qualitatively, this mechanism is due to the fact that at $H > H_{c1}$ a fluxon is in a magnetic potential well (see Fig. 7). In general, the depth of this well depends on the fluxon density and therefore needs to be calculated self-consistently. We first consider the simple case of $H \approx H_{c1}$, for which vortex-vortex interactions are negligible. The value of J_c is then determined by Eq. (20) obtained from the condition of disappearance of the surface barrier. Taking account of Eqs. (17) and (18), we get

$$J_c = \frac{c\phi_0}{16\pi d\lambda^2\alpha}[\cos^{-1}\sqrt{\alpha} - \sqrt{\alpha(1-\alpha)}] , \tag{39}$$

where

$$\alpha(d) = H_m/H_{c1} = (\pi^2/8)[\ln(d/\xi)+\gamma]^{-1} .$$

For $d=\lambda/2=120$ nm and $\xi=4.6$ nm, formula (39) yields $J_c=6\times10^6$ A/cm^2 at $H \approx H_{c1}(d)=0.3$ T [see Eq. (18)]. The calculated J_c is about $0.2J_d$, which sits between two experimental values, $J_c=10^7$ A/cm^2 and $J_c=3\times10^6$ A/cm^2 at $H=0$ and 1 T, respectively (see Fig. 3). Therefore, the magnetic surface pinning (unlike the bulk one) can provide very high values of J_c at $H \sim H_{c1}$ which turn out to be comparable to J_d for our nonprocessed Nb-Ti films at $d \leq \lambda/2$ (see also Ref. 52).

As has been already mentioned, the single-vortex critical current density $J_c(H)$ given by Eq. (20) increases with H due to the increase of the depth of the magnetic potential well $G_0(x_0)$ (Fig. 7).[32] However, when taking account of vortex-vortex interactions, the critical current density $J_c(H)$ experiences sharp drops each time when a new vortex row appears in the film upon increasing H.[43] This can manifest itself in a nonmonotonic low field dependence of $J_c(H)$, which has indeed been observed in LTS thin films.[11,12,53]

The surface pinning of the dense vortex structure in the field region $H_{c1} \ll H \ll H_{c2}$ was discussed by Shmidt.[32] In this case the intervortex repulsion strongly reduces the depth of the well in Fig. 7, which ultimately results in J_c of the order of that predicted by Eq. (39). Qualitatively, this result can be obtained by considering the following balance of two opposite forces which act on a vortex at the film surface. The first force

$$f_m = -\partial G_0/\partial x_0 = -H\phi_0 d/8\pi\lambda^2$$

is caused by the London screening currents. It is directed toward the film center (when calculating f_m we neglected a contribution of the fluxon self-energy given by the first term in Eq. (15) which is small at $H \gg H_{c1}$). The second

force $f_L = J\phi_0 N(H)/c$ is due to the transport current which pushes the vortex toward the surface. Here $N(H) \simeq Hd^2/\phi_0$ is a number of fluxons within the effective range of the vortex interaction ($r < d$), the factor $N(H)$ taking account of the fact that the vortex at the surface also experiences the elementary Lorentz forces applied to fluxons inside the film. By equating f_m to f_L, we obtain the critical current density $J_c \sim c\phi_0/8\pi\lambda^2 d$, which, within an accuracy to numerical coefficients of order of unity, coincides with Eq. (39) and the result of Ref. 32. Therefore, the magnetic surface pinning can provide high-J_c values in a wide field region $H_{c1} < H \ll H_{c2}$. In addition, this mechanism gives a $1/d$ dependence of J_c which is in agreement with our experimental data presented in Fig. 5.

As pointed out by Clem,[42] the interaction of fluxons with Meissner screening currents leads to their repulsion from the surface, which, in turn, may give rise to a vortex-free surface layer. This can result in a nonuniform distribution of the transport current density across the film, since the local $J_c(x)$ in the vortex-free regions is limited only by J_d, which is generally much higher than any J_c associated with the pinning of fluxons in the film. Such a vortex-free surface layer was observed in recent computer simulations of fluxon penetration into a superconducting slab.[54]

Similar surface effects can be due to the above-discussed nonuniformity of the intervortex forces which vanish at the film surface. This can also cause a nonuniformity of the local value of $J_c(x)$ across the film, since the vortex interaction at the surface is much weaker than in the bulk. Employing the above arguments of the collective pinning model, we can therefore conclude that the single-vortex pinning which result in the maximum J_c, first arises at the surface. This can manifest itself in the enhanced surface component of $J_c(x)$, even if pinning centers are uniformly distributed across the sample. An analogous effect can occur in bulk superconductors as well in the case of H parallel to the surface, which may pertain to the observed increase of $J_c(x)$ at the surface of bulk superconductors.[1]

V. DISCUSSION

Our results indicate that the film geometry can strongly affect both the absolute values and the orientational dependence of $J_c(\varphi)$. This effect is especially pronounced in thin films with $d < \lambda$ in parallel field for which J_c increases as d decreases, reaching about 20–30 % of J_d in the $\lambda/2$ and $\lambda/4$ films. Here the critical current density $J_{c\parallel}(d)$ in parallel field exhibits a stronger dependence on d than $J_{c\perp}(d)$ in perpendicular field. This manifests itself in the fact that $J_{c\parallel}(d) \ll J_{c\perp}(d)$ for thicker films, but $J_{c\parallel}(d) \gg J_{c\perp}(d)$ for thinner films, the crossover being observed at $d \approx 2\lambda$. It should be emphasized that we have specially chosen the isotropic Nb-Ti with weak bulk pinning in order to eliminate any intrinsic pinning and reveal the effect of the film geometry. Nevertheless, despite a degradation of T_c at $d < \lambda$, the J_c values turn out to be higher than those obtained by Cooley *et al.*[30] ($J_c \sim 3$–5 % of J_d) for the best optimized bulk Nb-Ti after the processing which gives rise to α-Ti precipitates.

The angular dependencies of $J_c(\varphi)$ exhibit strong peaks in parallel field, the amplitude of the peak increasing as d decreases. Notice that the dependences $J_c(\varphi)$ for our isotropic Nb-Ti films look remarkably similar to those observed on high-T_c thin films,[13–18] although in our case the contribution from the intrinsic pinning, to which such a behavior has been entirely ascribed so far, is absent. Instead, we obtained a significant geometrical effect which leads to a characteristic cusp in $J_c(\varphi)$ about $\varphi = 90°$ which can be well described by the power dependence $J_c \propto 1/|\varphi - 90°|^{0.42}$ (see, Fig. 2). This correlates with the results obtained on high-T_c films[13–18] and turns out to be rather close to the prediction of the intrinsic pinning model, $J_c \propto 1/|\varphi - 90°|^{1/2}$ at $|\varphi - 90°| \ll 1$ (Ref. 4) [see also Refs. 55–57, where the $J_c(\varphi)$ dependence was considered in terms of pinning of vortex kinks in the framework of the collective pinning approach]. Hence it follows, that the intrinsic pinning, although being important for highly anisotropic bulk HTS (see, e.g., Ref. 58), is not the only mechanism which can account for the observed orientational dependence of $J_c(\varphi)$. Our results show that at $d < \lambda$ the sample geometry can also play an important role in the forming of the $J_c(\varphi)$ dependence and therefore should be taken into account when analyzing experimental data on $J_c(\varphi)$ of thin films. For example, the sharp peaks in $J_c(\varphi)$ observed on $Bi_2Sr_2CaCu_2O_{8-x}$,[13] $Bi_2Sr_2Ca_2Cu_3O_{8+x}$ ($\lambda \approx 250$ nm,[17] and $YBa_2Cu_3O_{7-x}$ ($\lambda \approx 150$ nm) (Ref. 16) epitaxial films were measured on the films having thicknesses much smaller or of the order of λ ($d = 100$–300, 40–100, and 10–100 nm, respectively). At the same time, some features of the observed angular dependences $J_c(\varphi)$ for our Nb-Ti films differ from those of HTS; for instance, the data shown in Figs. 1 and 2 do not obey the scaling law $J_c(B,\varphi) = J_c(B\cos\varphi, 0)$ often observed on HTS films.[13,59,60] Such a scaling is believed to be due to the intrinsic pinning in highly anisotropic layered HTS.

Our interpretation of these results is based on the above-addressed peculiarities of the vortex behavior in thin films in parallel and perpendicular fields. First we notice that within the collective pinning theory, the values $J_{c\parallel}$ and $J_{c\perp}$ at $\lambda \ll d < L_c$ are proportional to the second and the first powers of the pinning strength parameter W, respectively [see Eqs. (36) and (38)], whereas the surface magnetic pinning gives a small contribution to the total I_c. Hence it follows that $J_{c\perp} > J_{c\parallel}$ in the case of a weak bulk pinning, which does correspond to our data for thick ($d \gg \lambda$), weak pinning Nb-Ti films (see Figs. 3 and 5). However, the relationship between $J_{c\parallel}$ and $J_{c\perp}$ reverses as d decreases below λ with $J_{c\parallel}$ reaching about $50J_{c\perp}$ for the $\lambda/4$ film . We believe that this is due to qualitatively different mechanisms of critical current control for parallel and perpendicular orientations at $d < \lambda$. For instance the experimental $J_{c\perp}$ did not undergo any qualitative change as d became smaller than λ; this is in agreement with the 2D collective pinning model which predicts that $J_{c\perp}$ should be proportional to the pinning strength parameter W and inversely proportional to the film thickness if $d < L_c$, where $L_c \gg d$ in the case of weak

bulk pinning [see Eqs. (32), (33), and (38)].

By contrast, we have found both experimentally and theoretically that the value $J_{c\parallel}$ is strongly affected by the film geometry, since at $d<\lambda$ the film becomes almost magnetically transparent. This gives rise to an increase of H_{c1} and the surface barrier, which, both act to enhance the field range, where J_c is mostly due to Meissner currents and thereby is of order of J_d [see Eq. (28)]. Above H_{c1}, the $J_{c\parallel}$ value is determined by flux pinning which is also strongly enhanced by the effect of the film geometry. This is due to the drop of the tilt and compression elastic moduli c_{44} and c_{11} as a result of the decreased range of the intervortex repulsion at $d<\lambda$. Such a "softening" of the vortex structure at $d<\lambda$ leads to a considerable growth of the bulk component of $J_{c\parallel}$ due to the better matching of the fluxons to even weak pinning potentials. This ultimately changes the mechanism of bulk pinning, giving rise to a crossover between the collective and single-vortex pinning below a critical thickness d_c. However, despite the increase of $J_{c\parallel}$ in the single-vortex regime, the bulk pinning in our films seems to be not strong enough to account for the high values of $J_{c\parallel}$ for $d=\lambda/2$ and $\lambda/4$. Indeed, this component of $J_{c\parallel}$ in the single-vortex regime weakly depends on the film geometry and thereby cannot exceed J_c for the bulk unoptimized Nb-Ti at $H\sim H_{c1}$. Since, however, the low-field $J_c(H)$ for the nonprocessed Nb-Ti is about 2–3 orders of magnitude smaller than J_d (Ref. 3) (see also Fig. 3), the core pinning cannot account for the observed high values of $J_{c\parallel}\approx 0.2-0.3J_d$ in our $\lambda/2$ and $\lambda/4$ films.

At the same time, the above calculations indicate that the surface magnetic pinning can provide $J_{c\parallel}$ of order J_d in the wide field region $H_{c1}<H\ll H_{c2}$ if the film thickness becomes smaller than $\lambda/2$. As was shown in the previous section, this mechanism which is entirely due to the film geometry gives a main contribution to $J_{c\parallel}$ at $d<\lambda$ and indeed allows one to account for the high $J_{c\parallel}$ values in our $\lambda/2$ and $\lambda/4$ films. In addition, the surface magnetic pinning gives rise to a $1/d$ dependence of $J_{c\parallel}$ which is also in agreement with our experimental data shown in Fig. 5.

Therefore, at $d<\lambda$, the surface pinning can result in $J_{c\parallel}$ of order J_d, unlike the value $J_{c\perp}$ for perpendicular orientation which remains proportional to the parameter W which characterizes the weak bulk pinning in our samples. These arguments allow one to account for the extremely high $J_{c\parallel}$ values which we observed in $\lambda/4$ and $\lambda/2$ thick films, despite the absence of α-Ti precipitates and the much smaller $J_{c\perp}$ values which should be determined by weak bulk pinning produced by the columnar grain boundaries which are the principal pinning centers in our unoptimized Nb-Ti films.

ACKNOWLEDGMENTS

We are grateful to J. E. Nordman of the University of Wisconsin for the use of a sputtering system for the production of the second film set. We also thank A. A. Abrikosov, J. R. Clem, K. E. Gray, and V. M. Vinokur for useful discussions. This work has been supported by the Department of Energy, Division of High Energy Physics (G.S., E.K., A.G., and D.C.L.) and the Electric Power Research Institute (A.G., R.J., and D.C.L.).

APPENDIX

As follows from Eqs. (4) and (7) the field $B(x,y)$ can be presented in the form

$$B(x,y)=\frac{\phi_0}{4\pi\lambda^2}\int_{-\infty}^{\infty}\frac{\cos q(u-u_0)}{g\sinh g}[\cosh g(1-|v-v_0|)-\cosh g(v+v_0)]dq\ , \tag{A1}$$

where $q=kd$, $u=y/d$, $v=x/d$, $g=(q^2+\epsilon^2)^{1/2}$, and $\epsilon=d/\lambda$. For thin films ($d\ll\lambda$), the main contribution to the integral in Eq. (A1) comes from $q\sim 1$. This allows us to set $\epsilon=0$ in Eq. (A1), which is equivalent to the replacement $p=(1/\lambda^2+k^2)^{1/2}=|k|$ in Eq. (6). Then Eq. (A1) becomes

$$B(x,y)=\frac{\phi_0}{2\pi\lambda^2}\int_0^{\infty}dk\frac{\cos k(y-y_0)}{k\sinh kd}[\cosh k(d-|x-x_0|)-\cosh k(x+x_0)]\ . \tag{A2}$$

This formula gives an integral representation of the Green function of the Laplace equation

$$\lambda^2\nabla^2 B=-\phi_0\delta(\mathbf{r}-\mathbf{r}_0) \tag{A3}$$

with the boundary conditions $J_x(\pm d/2,y)=0$. An evaluation of the integral in Eq. (A2) (see, e.g., Ref. 36) results in formula (8) which is an exact single-vortex solution of Eq. (A3). By differentiating Eq. (8) we calculate the components of the current density $J_x=(c/4\pi)\partial B/\partial y$ and $J_y=-(c/4\pi)\partial B/\partial x$, which yields

$$J_x=-\frac{c\phi_0}{16\pi\lambda^2 d}\left[\frac{\sinh\frac{\pi}{d}(y-y_0)}{\cosh\frac{\pi}{d}(y-y_0)-\cos\frac{\pi}{d}(x-x_0)}-\frac{\sinh\frac{\pi}{d}(y-y_0)}{\cosh\frac{\pi}{d}(y-y_0)+\cos\frac{\pi}{d}(x+x_0)}\right], \tag{A4}$$

$$J_y=\frac{c\phi_0}{16\pi\lambda^2 d}\left[\frac{\sin\frac{\pi}{d}(x-x_0)}{\cosh\frac{\pi}{d}(y-y_0)-\cos\frac{\pi}{d}(x-x_0)}+\frac{\sin\frac{\pi}{d}(x+x_0)}{\cosh\frac{\pi}{d}(y-y_0)+\cos\frac{\pi}{d}(x+x_0)}\right]. \tag{A5}$$

As follows from Eq. (A4), the normal component $J_x(x)$ vanishes at the film surface, $x=\pm d/2$.

Now we estimate a correction to Eq. (8) which comes from the bulk London screening which is neglected in

Eqs. (A2) and (A3). By expanding the Eq. (A1) in power series in $\epsilon^2=d^2/\lambda^2\ll 1$, we obtain the correction $\delta B(x,y)$ to Eq. (A2) proportional to ϵ^2. For instance, for the vortex being in the center of the film, the value $\delta B(0)$ at the core ($x=x_0=0$, $y=y_0=0$) is given by

$$\delta B(0)=\frac{\phi_0 d^2}{8\pi\lambda^4}\int_0^\infty \frac{dq}{q^2}\left[\frac{1}{\cosh^2 q}-\frac{\tanh q}{q}\right]. \quad \text{(A6)}$$

This integral converges, therefore at $d\ll\lambda$ the contribution from the London screening, $\delta B(0)$ is of order $\phi_0 d^2/4\pi\lambda^4$, which is negligible as compared to

$$B(0)\sim(\phi_0/2\pi\lambda^2)\ln(d/\xi)$$

given by Eq. (8).

[1]A. M. Campbell and J. E. Evetts, Adv. Phys. **21**, 1191 (1972).

[2]A. I. Larkin and A. Yu. Ovchinnikov, J. Low Temp. Phys. **34**, 409 (1979).

[3]D. C. Larbalestier and A. W. West, Acta Metall. **32**, 1871 (1984); D. C. Larbalestier, Physics Today, **44**(6), 74 (1991).

[4]M. Tachiki and S. Takachashi, Solid State Commun. **70**, 291 (1989); **72**, 1083 (1989).

[5]T. L. Hylton and M. R. Beasley, Phys. Rev. B **41**, 11 669 (1990).

[6]B. Oh, M. Naito, S. Arnason, P. Rosenthal, R. Barton, M. R. Beasley, T. H. Geballe, R. H. Hammond, and A. Kapitulnik, Appl. Phys. Lett. **51**, 11 (1987).

[7]J. Mannhart, P. Chaudhari, D. Dimos, C. C. Tsuei, and T. R. McGuire, Phys. Rev. Lett. **61**, 2476 (1988).

[8]B. Roas, L. Schultz, and G. Enders, Appl. Phys. Lett. **53**, 1557 (1988).

[9]K. Watanabe, T. Matsushita, N. Kobayashi, H. Kawabe, E. Aoyagi, K. Hiraga, H. Yamane, H. Kurosawa, T. Hirai, and Y. Muto, Appl. Phys. Lett. **65**, 1490 (1990).

[10]H. Jiang, Y. Huang, H. How, S. Zhang, C. Vittoria, A. Widom, D. B. Chrisey, J. S. Horwitz, and R. Lee, Phys. Rev. Lett. **63**, 1785 (1991).

[11]J. Sutton, Proc. Phys. Soc. **87**, 791 (1966).

[12]T. Yamashita and L. Rinderer, J. Low. Temp. Phys. **24**, 695 (1976).

[13]B. Roas, L. Schultz, and G. Saemann-Ischenko, Phys. Rev. Lett. **64**, 479 (1990); P. Schmitt, P. Kummeth, L. Schultz, and G. Saemann-Ischenko, *ibid.* **67**, 267 (1991).

[14]D. K. Christen, C. E. Klabunde, R. Feenstra, D. H. Lowndes, D. Norton, J. D. Budai, H. R. Kerchner, J. R. Thompson, L. A. Boatner, J. Narayan, and R. Singh, Physica C **165&166**, 1415 (1990).

[15]K. Watanabe, S. Awaji, N. Kobayashi, H. Yamane, T. Hirai, and Y. Muto, J. Appl. Phys. **69**, 1543 (1991).

[16]Y. Iye, T. Terashima, and Y. Bando, Physica C **177**, 393 (1991); **184**, 362 (1991).

[17]K. Endo, H. Yamasaki, S. Misawa, S. Yoshida, and K. Kajimura, Nature **355**, 327 (1992); H. Yamasaki, K. Endo, Y. Nakagawa, M. Umeda, S. Kosaka, S. Misawa, S. Yoshida, and K. Kajimura, J. Appl. Phys. **72**, 2951 (1992).

[18]S. Labdi, H. Raffy, O. Laborde, and P. Monceau, Physica C **197**, 274 (1992).

[19]I. K. Schuller, J. Guimpel, and Y. Bruynseraede, MRS Bull. **15**(2), 29 (1990).

[20]Y. Kuwasawa, T. Tosaka, A. Uchiyama, S. Matuda, and S. Nakano, Physica C **175**, 187 (1991); T. Nojima, M. Kinoshita, S. Nakano, and Y. Kuwasawa, *ibid.* **206**, 387 (1993).

[21]M. Hawley, I. D. Raistrick, J. G. Beery, and R. J. Houlton, Science **251**, 1587 (1991).

[22]Ch. Gerber, D. Anselmetti, J. G. Bednortz, J. Mannhart, and D. G. Schlom, Nature **350**, 279 (1991); J. Mannhart, D. Anselmetti, J. G. Bednortz, Ch. Gerber, K. A. Muller, and D. G. Schlom, Supercond. Sci. Technol. **5**, S125 (1992).

[23]P. H. Kes and C. C. Tsuei, Phys. Rev. Lett. **47**, 1930 (1981); Phys. Rev. B **28**, 5126 (1983).

[24]R. Wordenweber and P. H. Kes, Phys. Rev. B **34**, 494 (1986).

[25]E. H. Brandt, J. Low Temp. Phys. **64**, 375 (1986).

[26]N.-C. Yeh, Phys. Rev. B **41**, 4850 (1990).

[27]J. Pearl, Appl. Phys. Lett. **5**, 65 (1964).

[28]M. Tinkham, *Introduction to Superconductivity* (McGraw-Hill, New York, 1985).

[29]A. A. Abrikosov, *Fundamentals of the Theory of Metals* (North-Holland, Amsterdam, 1988).

[30]L. D. Cooley, P. D. Jablonski, P. J. Lee, and D. C. Larbalestier, Appl. Phys. Lett. **56**, 2284 (1991).

[31]A. A. Abrikosov, Zh. Exp. Teor. Fiz. **46**, 1464 (1964) [Sov. Phys. JETP **19**, 988 (1964)].

[32]V. V. Schmidt, Zh. Exp. Teor. Fiz. **57**, 2095 (1969) [Sov. Phys. JETP **30**, 1137 (1970)]; **61**, 398 (1971) [**34**, 211 (1972)].

[33]A. I. Rusinov and G. S. Mkrtchyan, Zh. Exp. Teor. Fiz. **61**, 773 (1971) [Sov. Phys. JETP **34**, 413 (1972)].

[34]V. V. Shmidt and G. S. Mkrtchyan, Usp. Fiz. Nauk **112**, 459 (1975) [Sov. Phys. Usp. **17**, 170 (1974)].

[35]E. B. Sonin, Europhys. Lett. **18**, 69 (1992).

[36]I. M. Gradshtein and I. M. Ryzhik, *Tables of Integrals, Series and Products* (Academic, New York, 1980).

[37]P. G. De Gennes, *Superconductivity of Metals and Alloys* (Benjamin, New York, 1966).

[38]T. P. Orlando and K. A. Delin, *Foundations of Applied Superconductivity* (Addison-Wesley, New York, 1991).

[39]As follows from detail calculations by C.-R. Hu [Phys. Rev. B **6**, 1756 (1972)], the bulk lower critical field is given by $H_{c1}=(\phi_0/4\pi\lambda^2)[\ln(\lambda/\xi)+0.497]$. On the other hand, in the London theory the value H_{c1} can be presented in the form $H_{c1}=(\phi_0/4\pi\lambda^2)[\ln(2\lambda/\xi)-C+\beta]$, where β is a parameter which accounts for the core energy, $\beta(\phi_0/4\pi\lambda)^2$, and $C=0.577$ is the Euler constant. Hence $\beta=0.497+C-\ln 2=0.38$.

[40]C. P. Bean and J. D. Livingston, Phys. Rev. Lett. **12**, 14 (1964); P. G. de Gennes, Solid State Commun. **3**, 127 (1965).

[41]J. R. Clem, R. P. Huebener, and D. E. Gallus, J. Low Temp. Phys. **12**, 449 (1973).

[42]J. R. Clem, in *Low Temperature Physics, LT-13*, edited by K. D. Timmerhaus, W. J. O'Sullivan, and E. F. Hammel (Plenum, New York, 1974), Vol. 3, p. 102.

[43]C. Carter, Can. J. Phys. **47**, 1447 (1969).

[44]S. Takacs, Czech. J. Phys. B **36**, 521 (1986); **38**, 1050 (1988).

[45]V. G. Kogan, Phys. Rev. Lett. **64**, 2192 (1990); V. G. Kogan, N. Nakagawa, and S. L. Thiemann, Phys. Rev. B **42**, 2631 (1990).

[46]A. M. Grishin, A. Yu. Martynovich, and S. V. Yampol'skii, Zh. Exp. Teor. Fiz. **97**, 1930 (1990) [Sov. Phys. JETP **70**, 1089 (1990)].

[47]A. I. Buzdin and A. Yu. Simonov, Physica C **175**, 143 (1991); A. Yu. Simonov and M. Yu. Moiseev, Phys. Rev. B **46**, 5556 (1992).

[48]E. H. Brandt, J. Low Temp. Phys. **26**, 709 (1977); **26**, 735 (1977); **28**, 263 (1977); **28**, 291 (1977); Phys. Rev. B **34**, 6514 (1986).

[49]M. Konczykowski, L. I. Burlachkov, Y. Yeshurun, and F. Holtzberg, Phys. Rev. B **43**, 13 707 (1991).

[50]M. V. Feigel'man and V. M. Vinokur, Phys. Rev. B **41**, 8986 (1990).

[51]L. Krusin-Elbaum, L. Civale, V. M. Vinokur, and F. Holtzberg, Phys. Rev. Lett. **69**, 2280 (1992).

[52]K. Yamafuji and Y. Mawatari (unpublished).

[53]A. Pruymboom, P. H. Kes, E. van der Drift, and S. Radelaar, Phys. Rev. Lett. **60**, 1430 (1988).

[54]R. Kato, Y. Enomoto, and S. Maekawa, Phys. Rev. B **47**, 8016 (1993).

[55]B. I. Ivlev, Yu. N. Ovchinnikov, and V. L. Pokrovsky, Europhys. Lett. **13**, 187 (1990); Mod. Phys. Lett. B **5**, 73 (1991).

[56]Yu. N. Ovchinnikov and B. I. Ivlev, Phys. Rev. B **43**, 8024 (1991).

[57]V. L. Pokrovsky, I. Lyuksyutov, and T. Nattermann, Phys. Rev. B **46**, 3071 (1992).

[58]Y. Iye, T. Tamegai, and S. Nakamura, Physica C **191**, 227 (1991); Y. Iye, I. Oguro, T. Tamegai, W. R. Datas, N. Motohira, and K. Kitazawa, *ibid.* **199**, 154 (1992).

[59]P. Schmitt, P. Kummeth, L. Schultz, and G. Saeman-Ischenko, Phys. Rev. Lett. **67**, 267 (1991).

[60]G. Jacob, P. Przyslupski, G. Stolzel, C. Tome-Rosa, A. Walkenhorst, M. Schmitt, and H. Adrian, Appl. Phys. Lett. **59**, 1626 (1991); G. Jakob, M. Schmitt, Th. Kluge, C. Tome-Rosa, P. Wagner, Th. Hahn, and H. Adrian, Phys. Rev. B **47**, 12 099 (1993).

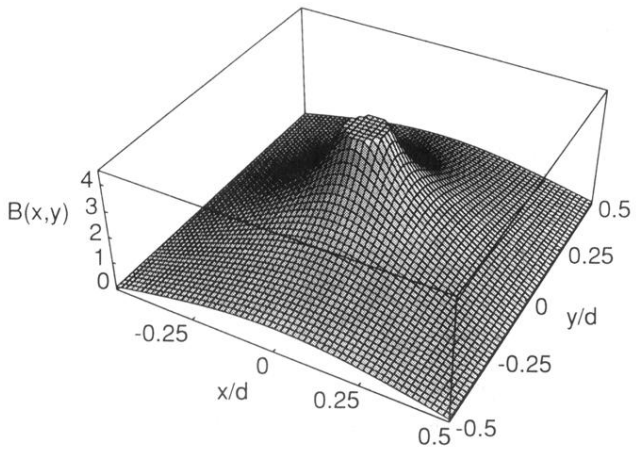

FIG. 6. Field distributions $B(x,y)$ in a fluxon calculated by means of Eq. (8) [$B(x,y)$ is measured in the units of $\phi_0/4\pi\lambda^2$].

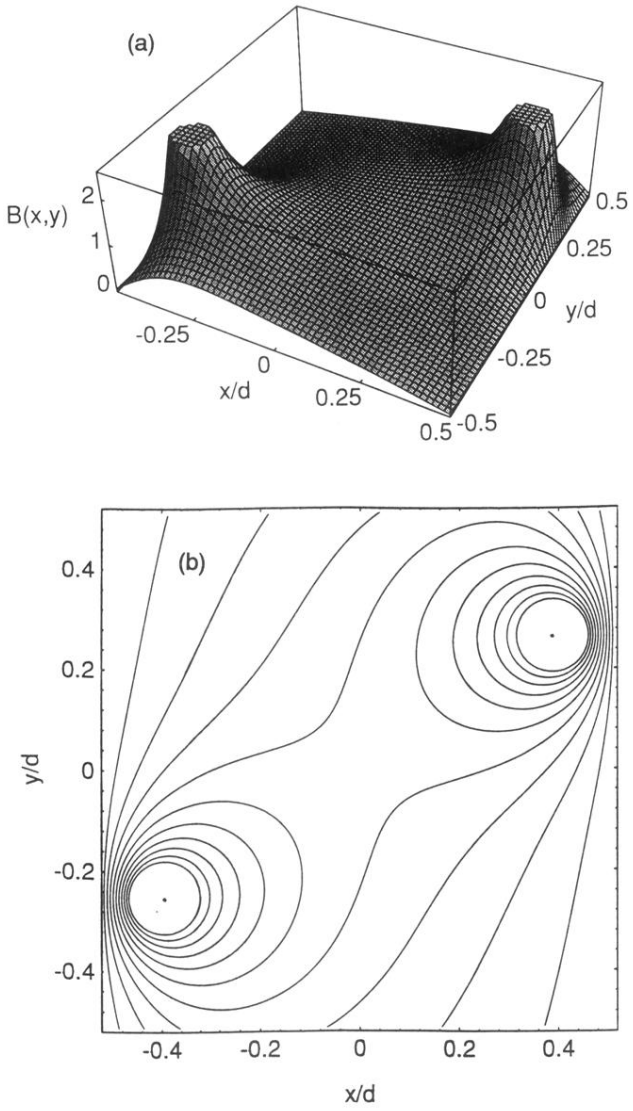

FIG. 9. Field distribution (a) and current lines (b) of a pair of fluxons located at $x_0 = \pm 0.4d$ and $y_0 = \pm 0.25d$ calculated by means of Eq. (8) [$B(x,y)$ is measured in the units of $\phi_0/4\pi\lambda^2$].